LANGMUIR Article
Cite This: Langmuir 2018, 34, 15335−15342
pubs.acs.org/Langmuir

Surface Characteristics Control the Attachment and Functionality of (Chimeric) Avidin

Dongkai Shao,[†] Kosti Tapio,[†] Sanna Auer,[‡] J. Jussi Toppari,[†] Vesa P. Hytönen,[‡] and Markus Ahlskog*[,†]

[†]Nanoscience Center, Department of Physics, University of Jyväskylä, Jyväskylä FI-40014, Finland

[‡]Faculty of Medicine and Life Sciences and BioMediTech, University of Tampere, and Fimlab Laboratories, Tampere FI-33520, Finland

Supporting Information

ABSTRACT: The physical adsorption (physisorption) of proteins to surfaces is an important but incompletely understood factor in many biological processes and is of increasing significance in bionanotechnology as well. Avidin is an important protein because of strong avidin−biotin binding, which has been exploited in numerous applications. We have undertaken thorough experimentation on the physisorption of avidin, to chemically different flat surfaces of Si and graphite and also to the curved version of the latter, on multiwalled carbon nanotubes (MWNTs) of different diameters. The difference in the behavior of avidin on Si versus graphite is drastic; on Si, avidin deposits as single globular tetrameric units and maintains functionality, whereas on graphite, it forms irregular networks of two-layer thick filaments, where the first layer has lost its biological activity. On MWNTs, avidin also deposits as one-dimensional formations, or stripes, but these appear to order in a perpendicular arrangement to the MWNT axis. A better understanding of protein−surface interactions is essential for the development of robust and reliable methods for biofunctionalization of materials. This work also provides insights into the importance of the nanoscale surface architecture.

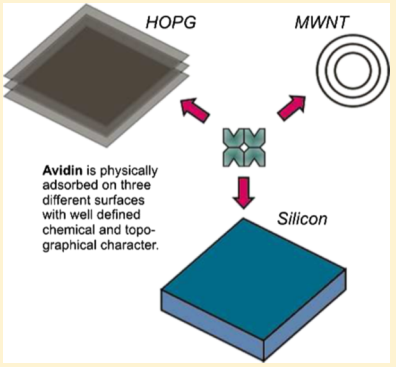

INTRODUCTION

Physical adsorption (physisorption) of proteins on solid surfaces is important in many biological processes. In bio- and nanotechnology, the phenomenon is of interest for biointerfaces, although the purpose is often to avoid physical adsorption of proteins to certain surfaces. On the other hand, in applications where a protein monolayer is needed, it is more common to resort to covalent linking, that is, chemical adsorption, of the protein to the surface. Covalent linking can ensure the desired orientation of the protein and thus preserve its functionality. However, the prevalence of chemical adsorption is one motivation for also studying physisorption of proteins, as the two can be difficult to separate from each other with absolute certainty.[1]

The complexity of proteins ensures that even though physisorption is simple to execute, it is difficult to investigate in a detailed level.[2−4]

Especially, the older experimental work on protein adhesion phenomena has been undertaken with techniques, such as ellipsometry and the quartz crystal microbalance, which at best can sense the formation of a monolayer but do not reach the single-molecule level.[5] The individual protein may severely change its conformational state upon interaction with the surface, and if the surface mobility is high, there is the possibility of complex pattern formation, which requires high-resolution imaging data in order to be investigated and understood.

There are a number of both theoretical and experimental atomic force microscopy (AFM) studies of individual protein deposition on surfaces such as Si[6,7] and graphite and graphene.[8−12] Yet, because of the complexity of the problem, many important aspects remain open issues.

Conventionally, in both applications and experimentation, one has used substrates whose surfaces are flat both on macroscopic and microscopic scales, such as silicon, certain oxides, mica, graphite, and so forth. For such surfaces, parameters that are of prime importance are surface energy, polarity, and charge. In addition to these, surface topography has rarely been a parameter in experiments, as in reality, it is difficult to have it under control at the nanometer scales that are most relevant for proteins. This does not mean that surface topography could not sometimes be a major factor. However, AFM allows the surface topography to be conveniently measured on those scales. Moreover, carbon nanotubes offer a practically realizable surface with a clean and well-defined curvature on that scale. Arc-discharge synthesized multiwalled carbon nanotubes (MWNTs) were the first type of carbon nanotubes discovered,[13] but are nowadays at the fringe of interest because of the abundance of carbon impurities and the unscalability of the synthesis method. Yet, they are of a high

Received: August 27, 2018
Revised: October 19, 2018
Published: November 6, 2018

quality and can provide a nearly perfect curved graphitic surface in a tube diameter range at least up to 20 nm.[14]

In this work, we have studied experimentally the physical adsorption of tetrameric avidin to different surfaces, a protein which is important both in current technology and in bionanotechnological research.

Avidins are well-known because of the superior strength of the noncovalent binding between avidin and biotin molecules, which is utilized in numerous applications such as for labeling, biofunctionalization, targeting, and delivery.[15] The majority of avidins are tetrameric proteins, and their functionality is lost if the tetramer is dissociated. In the applications and numerous research works where avidin or streptavidin has been used, usually, it has been covalently linked to a surface or to a nanoparticle. Therefore, despite being a commonly used protein, there is not much in the research literature on the physical adsorption properties of avidin.

The main elements of the experiments of this work are summed up in Figure 1. We use silicon (Si) and highly oriented pyrolytic graphite (HOPG) as smooth chemically different surfaces. A third substrate is the MWNT, which realizes testing of the effect of curvature on HOPG. We found fundamental and well-defined differences in the adsorption patterns of avidin depending on the surface characteristics. For applications, the important aspects are stability and functionality of the adsorbed protein molecule. The functionality of avidin−biotin binding in the monolayer scale avidin deposits was tested with biotinylated gold nanoparticles (b-AuNPs) and was found to work well under specific conditions.

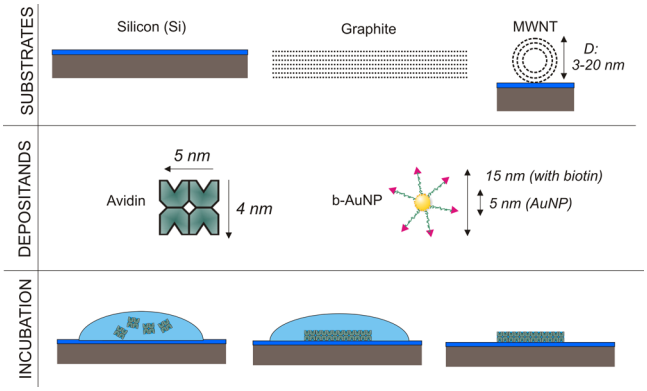

Figure 1. Essential elements of the experiments. First row: the substrates used for physical protein adsorption. Second row: the protein we study is avidin, which is a homotetrameric protein. b-AuNPs are used to test the functionality of avidin with respect to its ability to bind biotin. Third row: scheme for the simplest incubation technique of avidin on a surface, which is some of three mentioned above. A droplet of a solution of avidin is placed on a substrate, and allowed to stand there for a predetermined time. Physisorption of avidins takes place during this time, after which the droplet is blown away.

EXPERIMENTAL SECTION

Materials. Chimeric avidin has been obtained as a hybrid of chicken avidin and avidin-related protein 4 and produced in *Escherichia coli* using the method described earlier.[16] Chimeric avidin consists of four identical subunits with a molecular weight of 52.6 kDa per tetramer. It has extremely high thermal stability (melting temperature 111.1 °C). Two independent batches of chimeric avidin were used in the following experiments with very similar results. For the preparation of samples, phosphate-buffered saline (PBS) buffer was used for all experiments involving avidin and b-AuNPs. The composition of PBS buffer used is 0.8 g/L of NaCl, 0.2 g/L of KCl, 1.4 g/L of $Na_2HPO_4{\cdot}2H_2O$, and 0.2 g/L of KH_2PO_4. Deionized water was prepared with a Milli-Q ultrapure water system. b-AuNPs of 5 nm diameter (Figure 1) were purchased from Cytodiagnostics.[a] On average, there are around 40 biotin groups on each AuNP based on the surface area and biotin group density.

Sample Preparation. Precut 8 mm × 8 mm pieces of silicon wafer were cleaned from small particles by blowing with a carbon dioxide gas gun and then washing with acetone and isopropyl alcohol. The Si pieces were rendered hydrophilic or hydrophobic with reactive ion etching (RIE-Plus Oxford Instruments). The etching was done for 2 min at 30 °C and 300 W forward power. The flow parameters were 50 sccm O_2 for hydrophilic treatment and 50 sccm CHF_3 and 5 sccm O_2 for hydrophobic treatment. The hydrophilic treatment results, predominantly, in a thin layer of −OH groups on the silicon surface, similar to the conventional piranha treatment. The hydrophobic treatment removes the native silicon oxide on top of the silicon surface, which will leave pure silicon surface, which is hydrophobic. The surface of course immediately begins to reoxidize, but for the time required to perform the experiments, usually within an hour, the hydrophobic character will dominate. HOPG was purchased from Goodfellow Ltd. Fresh HOPG surfaces were used for the experiments and were obtained by simple cleaving of the piece of HOPG. The contact angle of a water droplet on both HOPG and hydrophobic silicon is c. 85°.

An arc-discharge synthesized MWNT material was used, which contains high-quality MWNTs, but also much graphitic carbon debris. The MWNTs were randomly distributed on Si/SiO_2 chips, with microlithographically fabricated 200 nm wide trenches, so that we could find tubes both on the solid surface and crossing the trenches. The diameter distribution of MWNTs was 2−20 nm, which means that usually a tube crossing a trench was mechanically rigid enough to be almost straight on the suspended part and to be able to stay so during imaging with AFM. Further details are given in the Supporting Information.

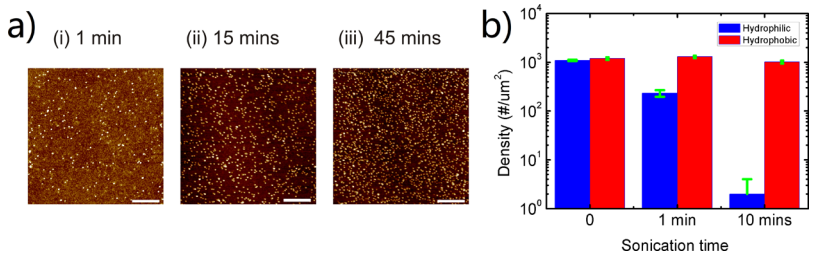

Figure 2. Deposition of avidin on silicon. (a) AFM images of avidin on hydrophobic surfaces, after incubation from 0.1 μM solution. The incubation times are indicated above the figures. Scale bar 200 nm. (b) To evaluate the attachment strength, the density of avidin (nr. per square micrometer) is displayed as a function of bath sonication time, on hydrophobic and hydrophilic surfaces that initially had a high concentration. The density was calculated on three different sites of the sample. The error bars indicate the deviations.

DOI: 10.1021/acs.langmuir.8b02855
Langmuir 2018, 34, 15335−15342

Physical adsorption of avidin was done by incubation (Figure 1). After appropriate conditioning of the substrate, a small droplet (usually 50 μL) of avidin solution was placed on it. The washing steps included three dd-H_2O immersions (1 min each) and blowing of air using a 1000 μL pipette three times. The sample was then dried with a nitrogen gas gun.

All the important results of this work are based on repeated experimentation. The presented sets of data of deposition on silicon and graphite are the results of multiple tests where we have tried out different concentrations, incubation times, and some other deposition parameters that are optimal for revealing the fundamental effects. The same applies for the work on MWNTs, but here, there are more practical difficulties, as the MWNTs exist in a distribution of diameters, that appear randomly in the deposited MWNT material. Therefore, each MWNT sample is, strictly speaking, unique. We have prepared a total of c. 50 individual MWNTs for the experiments described here, which was sufficient for us to obtain several samples around each diameter in the range of 2−20 nm. Another essential aspect is that arc-discharge grown MWNTs are of superior quality compared to ordinary chemical vapor deposition grown MWNTs.[17]

RESULTS AND DISCUSSION

Figure 2a shows the AFM images of the result of physical adsorption of avidin on the Si surface. The main observation is that avidin deposits as randomly placed globular clusters, presumably single tetramers on the silicon surface. As expected, the density of avidins on the surface increases with increasing solution concentration and incubation time. A close-up image of high density of avidin is shown in Figure 3. The

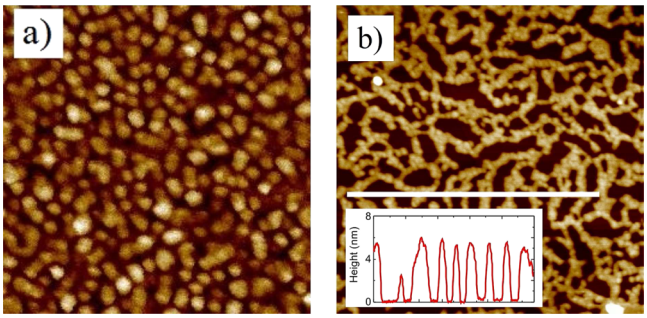

Figure 3. Dense avidin deposition on (a) Si (size 200 nm) and (b) graphite (size 1 μm). Inset: AFM height data along the line on the graphite figure.

hydrophilicity of silicon surface has little effect on the final deposition density of avidin. The highest density we found is around 6500 units per square micrometer at pH = 7 buffer.

The height of avidin on a silicon surface is around 2.5−3 nm, both on hydrophilic and hydrophobic surfaces. This is about half of the tetramer size of avidin in solution, as determined by X-ray diffraction.[18] It is rather obvious that crystallography supports a highly extended shape of the protein, which partially collapses on a surface, even if we preserve the major characteristics of the protein. We may thus claim that 2.5−3 nm is in fair agreement with the size of the functional core of the tetrameric protein (after drying the sample).

We found that the hydrophilicity of the Si surface affects the affinity of adsorbed avidin. This was tested with simple bath sonication. The graph of Figure 2b shows that the density of avidin on a hydrophobic surface nearly keeps constant for 10 min of sonication time, whereas on a hydrophilic surface, it drops very strongly, indicating loose attachment. Moreover, we used AFM imaging with the PeakForce mode (Bruker Icon) to adjust the peak force setpoint, the maximum force with which the oscillating tip is interacting with the surface. We found that we could move avidin on a hydrophobic surface with 30 nN as the peak force setpoint, whereas on a hydrophilic surface, 14 nN was sufficient, again indicating that avidin binding is tighter in the former case.

Figure 4 shows avidin on HOPG after incubation from 1 μM solution, in samples with different incubation times and with AFM profile height data. It is evident that, unlike on the Si surface, avidin has a strong tendency upon physical adsorption to aggregate into patterns on HOPG surfaces. After the shortest 30 s incubation, shown in the first image (i), avidins have formed separated irregular or slightly chain-like clusters. Some of these clusters appear to form linear assemblies, which most likely correspond to the omnipresent single-layer fault lines of a HOPG surface. The same phenomenon has been observed with other proteins.[19] A closer image of a typical avidin cluster is shown in the inset of Figure 4(i). The height of these irregular clusters is around 1.5−2 nm, which is lower than the individual avidin height on Si.

Figure 4(ii) shows the avidin patterns after a longer, 1 min incubation. There is a crucial difference to the previous figure: the pattern is essentially similar, but from the AFM height data, we can see that besides the 2 nm height, a second height level of around 4 nm appears. Our interpretation is that a second layer of avidin starts to form on top of the first deposited (mono-)layer, already slightly chain-like in appearance. In this case, the second, which we call a double layer, has not fully covered the first monolayer. In the third, 15 min incubation, all avidin structures are now around 4−5 nm in height, corresponding to the double-layer type of deposition.

Figure 3b shows how the avidin pattern on HOPG develops after a further increase of the incubation time. The chain structures, still having the same 4−5 nm height, get connected to form an irregular network. The size of the empty regions is in the 10−100 nm range. The width of the chain structures does initially correspond to what is expected from images with tip-convolution widening of a single avidin tetramer unit. The avidin deposits widen further upon increasing the time, an example of which is shown in Figure 7c.

Next, we move to arc-discharge MWNTs, which give us the opportunity to study deposition on curved graphite. Although the material contains amorphous carbon debris, the tubes themselves are of high quality, and by searching, one can find in selected locations MWNTs with few impurities within a micron scale area. Figure 5a shows an MWNT of diameter 10 nm before deposition. The AFM images reveal a smooth tube surface mostly absent of impurity particles or other deficiencies. More details are presented in the Supporting Information.

Figure 6 shows two suspended MWNTs of diameter 16 and 17 nm, after avidin deposition. A most interesting result is the character of avidin depositions, observed in these larger diameter MWNTs. The deposits have the form of stripes that are roughly perpendicular to the tube axis. Besides occasional differences, we did not observe any clear-cut evidence for different depositions of avidin on a suspended section compared to the nonsuspended parts. We conclude that possible effects of the suspension are masked by complicated local effects beyond our control.

Figure 5b,c shows tubes of smaller diameter, where the deposits are still present but their stripe-like character, as

DOI: 10.1021/acs.langmuir.8b02855
Langmuir 2018, 34, 15335−15342

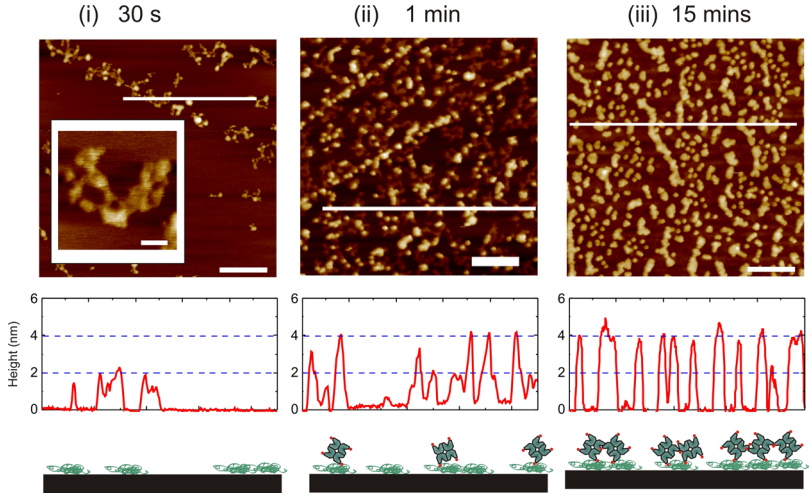

Figure 4. Avidin deposition on HOPG. The uppermost AFM images show the deposited avidin, after incubation in 1 μM solution for three different times. These times are indicated above the figures. Scale bars are 100 nm. (i) Closer image as the inset, with a scale bar of 20 nm. Below the AFM images are the extracted topographical height data (along the lines). Lowest is the schematic illustration of the suggested model for pattern formation by the avidins.

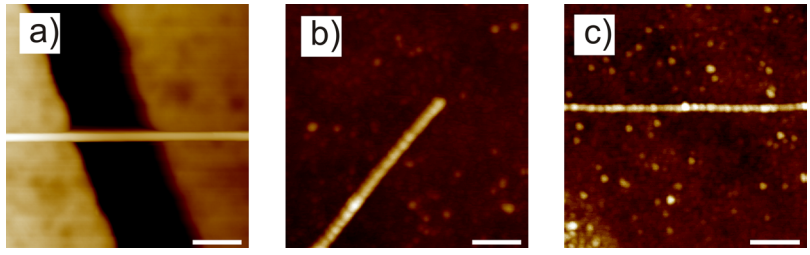

Figure 5. AFM images of the experiments with avidin deposition on MWNTs. (a) Suspended, intermediate-sized MWNT (D = 10 nm) before deposition. The tube is perfectly clean, within the resolution limit of AFM. (b) Avidin on MWNT with D = 5 nm. (c) Avidin on MWNT with D = 3 nm. In these smaller tubes, the MWNT diameter is close to the size of globular, folded avidin.

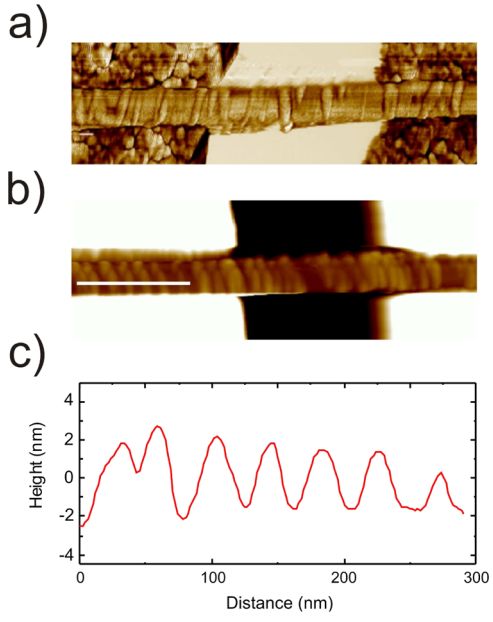

Figure 6. AFM images of avidin deposition on larger MWNTs. (a) Suspended MWNT with D = 16 nm and (b) suspended MWNT with D = 17 nm. The avidin is seen as stripes perpendicular to the tube axis. (c) Height profile along the line in (b).

observed with AFM, gradually vanishes. Besides the self-evident fact that there is no space for multiple proteins to link up into chains across the smallest tubes, it is, to a large extent, understandable as a technical imaging issue. The tip radius is typically around 10 nm and the tip apex is of course not truly spherical and is therefore unable to discern the real geometry of avidin deposition around the curvature of smaller diameter tubes. The height is measured as 2−5 nm, and we did not find a visible transition from single-layer to double-layer structures. Despite this inaccuracy, it is clear that the height corresponds to that on graphite. The separation between the stripes varies but is in the range 20−40 nm. Figure 6b demonstrates that the deposits can sometimes be very regularly spaced.

The last results of this work are the tests on the functionality of avidin deposits and on the ability of the surface-bound avidins to bind the b-AuNPs via the biotin coupling. Deposits of avidin on Si and HOPG were separately incubated with a solution of b-AuNP. In the case of avidin on Si, we present in the supplement the data images of incubation with b-AuNPs on avidin deposition. In this case, it was not easy to discriminate unambiguously between avidins complexed with b-AuNP and very possible sole b-AuNPs on the surface. However, the data implies that, on (hydrophobic) silicon, avidin has an affinity for b-AuNPs. The affinity is clearly greater than that of b-AuNP to bare silicon.

On HOPG, the results were less ambiguous and more interesting. We demonstrate that the distinctly different mono- and double-layer formations of avidin (Figure 4) have dramatically different affinities to b-AuNPs. We made b-AuNP incubation tests on these two formations, and

DOI: 10.1021/acs.langmuir.8b02855
Langmuir 2018, 34, 15335−15342

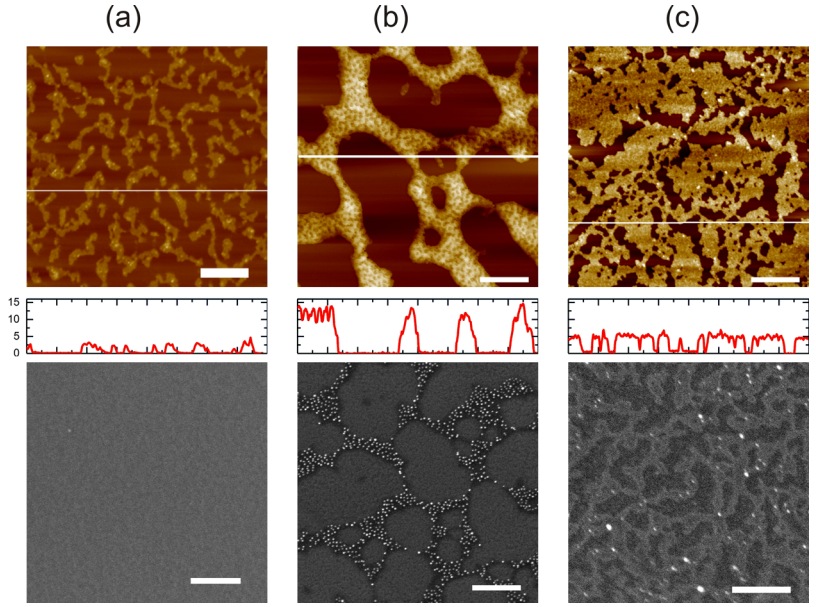

Figure 7. Testing functionality of three different avidin layers on HOPG by incubation with b-AuNPs and subsequent imaging. For each case, on top is an AFM image and below it is the height profile. Lowest is a SEM image. (a) Avidin monolayer; (b) avidin double layer; and (c) d-biotin-blocked double layer. Scale bar 200 nm.

additionally on a third one, which was a double layer made from biotin-blocked avidin. This third type is for control purpose only, as such avidin cannot link to b-AuNPs. The results of incubation tests on these three systems are presented with AFM and scanning electron microscopy (SEM) images in Figure 7, where each column of images corresponds to one of the above-mentioned systems.

The first and second columns of Figure 7 show results of deposition of b-AuNP on the mono- and double layers, respectively. In a single column, above is an AFM image with a height data profile and below these is an SEM image. It is strikingly clear that on the presumed unfolded/denatured single-layer chain structure (first column), there is little affinity to b-AuNPs, as especially the SEM images reveal (Figure 7a) the absence of any gold particles. As opposed to this, the double-layer structure (second column) efficiently attracts b-AuNPs. The third column contains images of a double layer made from biotin-blocked avidin (Figure 7c). The affinity for b-AuNP is negligible, which then confirms avidin−biotin linking as the mechanism behind affinity to the double layer.

We have shown that avidin deposits in very specific and different ways depending on the characteristic surface. On silicon, avidin deposits as isolated globular clusters, and this individual character remains discernible even at the highest densities of the deposits (Figure 3). The behavior is in two ways starkly different on graphite. First, no globules were seen. The first single proteins, imaged after the shortest incubation times (Figure 4(i)), show a tendency to spread along the graphite surface. Second, after a little longer incubation, the avidin forms irregular chain structures. On the MWNTs, similar one-dimensional (1D)-like chain formations are found as on graphite, which are called "stripes", and are organized roughly perpendicular to the tube axis. We must relate these data to general results on protein physisorption, as most of the molecular dynamics simulations on avidin have focused on its interaction with biotin[20−22] and have ignored issues related to bulk surfaces.

The individual globular clusters on Si are interpreted as single avidin tetramers. The measured height, ∼2.5 nm, is clearly lower than what would be implied from the solution-phase crystallographic data (5 nm × 5 nm × 4 nm), which is expected because of the immersed water and fully extended protein conformation in the latter. Otherwise, there is no indication in the AFM data on the decomposition of avidins on a silicon surface. Moreover, the height is independent of its hydrophilic/hydrophobic state, whereas hydrophilicity seems to matter with respect to the affinity of avidin to the silicon surface, a result in agreement with the well-documented adherence of proteins to hydrophobic surfaces.[2]

For graphite, concerning the individual behavior, both experimental and theoretical work are in line with our results. In ref 23, simulation revealed that avidin and graphene can form stable complexes primarily via hydrophobic forces and suggested conformational rearrangement near the surface. However, this work uses only one monomer of avidin, while we have utilized the biologically more relevant tetrameric form. The recent work of Barinov et al.[24] obtained quite solid results by investigating three different proteins on fresh and hydrophilically modified graphite. The results confirm that proteins commonly tend to collapse/denature on a plain graphite surface, which is what we described as spreading in the AFM data. The work also makes the case that confusing results are easily obtained if the graphite surface has significant contamination. Thus, the spreading of avidin on graphite that we observed in the very first deposits (Figure 4(i)) is supported by other works.

The other big difference between Si and graphite is that on the former, the avidin deposits solely as single globular proteins, while agglomeration dominates in graphite. The competition between these two mechanisms is a familiar issue in studies on physical adsorption of proteins.[3,4] Single-protein deposition has been quantitatively explained by Langmuir adsorption and/or randomized sequential adsorption theories, which depict the adsorption process to consist of individual proteins that stochastically land on empty slots on the surface.

DOI: 10.1021/acs.langmuir.8b02855
Langmuir 2018, 34, 15335−15342

An essential feature is that the protein molecules normally are charged and thus repel each other at close distances, leading to different maximum packing densities. In this work, the avidin monolayer has, at saturation coverage, a density of around 6000 per micrometer squared (500 Ru). This is about 20% of the highest reported chemical adsorption density of avidin on biotin-functionalized surfaces (2800 Ru).[25] A possible explanation could be that avidin in PBS bears a net positive surface charge (pI = 9.5 > pH = 7 buffer), causing interprotein repulsion.

The very different avidin patterns on graphite result from an agglomeration process. Similar AFM studies have been reported previously with ezrin[26] and fibrinogen.[27] Fibrinogen is present in blood and plays a key role in the coagulation process, whereby physical adhesion is of special relevance. It was shown[27] that fibrinogen can deposit (on polyethylene crystals) as individual proteins or as 1D, single-molecule thick chains, depending on solution parameters such as pH value. It was argued that the interplay between protein−protein interaction, surface diffusion, and surface−protein interaction determines whether aggregation occurs, and the weight of different factors can be tuned. Thus, the tendency of proteins to form monolayered chain structures under specific conditions, the same as in our case with avidin on graphite, has been well demonstrated, although a solid theoretical understanding is still lacking. The exact mechanism of how the bilayered chain structures (Figure 4(ii)) of avidin on graphite are formed is not clear. Our observations point to a two-stepped formation process, where the deposition of the first layer is strongly accompanied by denaturation and protein unfolding and this layer having a small height. Seemingly, this first layer is strongly adhering to the next avidin still in the solution phase, leading to the formation of the bilayer structure (Figure 4a).

On the MWNTs, the organized structure of avidin stripe deposition could be concluded from those tubes that were large enough, that is, had a radius not smaller than the AFM tip radius. The image data from smaller tubes did not allow the same resolution but apart from that is not in contradiction with the data from the larger tubes. The distance between the stripes is typically 20−40 nm and could be very regular (Figure 6b), which hints at a mechanism with a repulsive force between the avidin stripes, as they deposit on the MWNT.

In a few previous works,[28−30] carbon nanotubes and different proteins have been mixed together to enable the water solubility of the tubes. These works have demonstrated the affinity of carbon nanotubes toward proteins. However, most of them use only single-walled nanotubes (SWNTs), with diameter 1−2 nm. More or less casual AFM imaging of protein-functionalized carbon nanotubes has been reported, but to our knowledge, there is no previous AFM imaging data that reveal the actual organization patterns of proteins on nanotubes. There are at least two reports of transmission electron microscopy (TEM) high-resolution imaging of proteins on the MWNT surface, despite that the TEM imaging of proteins is seriously hampered by the low visibility as they consist of light atoms. Balavoine et al.[31] reported of streptavidin on MWNTs while Ling et al.[32] reported of a recognition protein (C1q) on the MWNT. Both works are on arc-discharge MWNTs, as in our case. Also, in both cases, perpendicular or helical arrangement of the protein was observed.

That there are very few works on the TEM imaging of proteins physically adsorbed onto high-quality arc-discharge synthesized MWNTs is understandable because of the multiple problems involved both in sample preparation and the imaging technique. Our AFM results support the tentative conclusion from the above-mentioned two TEM works, where certain proteins tend to arrange perpendicular to the tube axis. The fact that avidin on graphite forms a random network built up by chain formations, while on MWNTs, the corresponding stripes are organized perpendicular to the tube axis, implies that the avidin deposition energetically favors some degree of curvature upon adsorption to a graphitic surface.

De Leo et al.[12] have reviewed, mainly from the simulation point of view, the issue of proteins interfacing with graphitic nanomaterials, including carbon nanotubes. Besides the intermolecular forces, a crucial factor is what is called shape complementarity, which means that certain proteins have a concave-shaped section, which has been shown to act as a docking site for fullerenes and SWNTs. Larger nanotubes, that is, MWNTs, have a smaller curvature and therefore shape complementarity may not be particularly effective. Yet, a few experimental[30] and theoretical[9] reports do claim increased affinity of proteins to MWNTs with an increasing MWNT diameter.

Finally, the pertinent question with protein assembly on surfaces is that of their functionality. Our results demonstrate a very specific behavior of avidin, as on graphite, the double layer exhibits capture of b-AuNP while the monolayer does not. The result was well confirmed by the blocking of the biotin sites in the double layer so that no b-AuNP was adsorbed. These findings suggest that the first avidin layer is unfolded and represents protein which has lost the biological function. The first layer then modifies the surface properties so that the second layer stays functional.

CONCLUSIONS

In conclusion, we have undertaken thorough experimentation on the physisorption of avidin to chemically different flat surfaces, Si and graphite, and also to the curved version of the latter, on high-quality MWNTs of different diameters. The difference between the behavior of avidin on Si and graphite is drastic, in that on Si, avidin deposits as single globular tetrameric units, while on graphite, spreading of avidin along the surface occurs and it also agglomerates in chain-like formations. Eventually, avidin on graphite forms irregular networks of two-layer thick filaments. The upper avidins of this double layer and the globular clusters on silicon exhibit preserved functionality with respect to biotin binding, whereas the first layer of avidin on graphite has lost its functionality. On MWNTs, avidin, also upon deposition, agglomerates into 1D formations as on graphite. However, as opposed to the irregular network appearance on graphite, the cylindrical nanometer-sized curvature favors ordering of avidin in a perpendicular and at best periodical arrangement to the MWNT axis. This work has significance within avidin−biotin technology and may facilitate the engineering of protein−surface interfaces in general.[33,34] Our study reveals some challenges associated with physisorption, but may also open avenues for exploitation of surface-induced effects. The phenomena of protein−surface interactions are still understood only partly, as simulation requires large computing power and the available experimental data are limited in quality. The relatively well-defined variation in the exper-

DOI: 10.1021/acs.langmuir.8b02855
Langmuir 2018, 34, 15335−15342

imental parameters of this work (surface chemistry and nanoscale topography) should help the field to make further advances.

■ ASSOCIATED CONTENT

Supporting Information

The Supporting Information is available free of charge on the ACS Publications website at DOI: 10.1021/acs.langmuir.8b02855.

MWNT material and deposition, surface characterization, and functionality of avidin on silicon (PDF)

■ AUTHOR INFORMATION

Corresponding Author

*E-mail: markus.e.ahlskog@jyu.fi. Phone: +358 (0) 407284358.

ORCID

J. Jussi Toppari: 0000-0002-1698-5591
Vesa P. Hytönen: 0000-0002-9357-1480
Markus Ahlskog: 0000-0003-3479-2619

Notes

The authors declare no competing financial interest.

■ ACKNOWLEDGMENTS

This work was financially supported by the Academy of Finland through projects 263526, 130900, and 283011 for J.J.T., 263540 and 290506 for V.P.H., and 263523 for M.A. We thank Harlan Barker for insightful comments for the manuscript.

■ ADDITIONAL NOTE

[a]www.cytodiagnostics.com.

■ REFERENCES

(1) Nel, A. E.; Mädler, L.; Velegol, D.; Xia, T.; Hoek, E. M. V.; Somasundaran, P.; Klaessig, F.; Castranova, V.; Thompson, M. Understanding biophysicochemical interactions at the nano-bio interface. *Nat. Mater.* **2009**, *8*, 543−557.

(2) Anand, G.; Sharma, S.; Dutta, A. K.; Kumar, S. K.; Belfort, G. Conformational Transitions of Adsorbed Proteins on Surfaces of Varying Polarity. *Langmuir* **2010**, *26*, 10803−10811.

(3) Rabe, M.; Verdes, D.; Seeger, S. Understanding protein adsorption phenomena at solid surfaces. *Adv. Colloid Interface Sci.* **2011**, *162*, 87−106.

(4) Kastantin, M.; Langdon, B. B.; Schwartz, D. K. A bottom-up approach to understanding protein layer formation at solid-liquid interfaces. *Adv. Colloid Interface Sci.* **2014**, *207*, 240−252 , Special Issue: Helmuth Möhwald Honorary Issue .

(5) Spaargaren, J.; Giesen, P. L. A.; Janssen, M. P.; Voorberg, J.; Willems, G. M.; van Mourik, J. A. Binding of blood coagulation factor VIII and its light chain to phosphatidylserine/phosphatidylcholine bilayers as measured by ellipsometry. *Biochem. J.* **1995**, *310*, 539−545.

(6) Sommerfeld, J.; Richter, J.; Niepelt, R.; Kosan, S.; Keller, T. F.; Jandt, K. D.; Ronning, C. Protein Adsorption on Nano-scaled, Rippled TiO2 and Si Surfaces. *Biointerphases* **2012**, *7*, 55.

(7) Nejad, M. A.; Mücksch, C.; Urbassek, H. M. Insulin adsorption on crystalline SiO_2: Comparison between polar and nonpolar surfaces using accelerated molecular-dynamics simulations. *Chem. Phys. Lett.* **2017**, *670*, 77−83.

(8) Zou, X.; Wei, S.; Jasensky, J.; Xiao, M.; Wang, Q.; Brooks, C. L., III; Chen, Z. Molecular Interactions between Graphene and Biological Molecules. *J. Am. Chem. Soc.* **2017**, *139*, 1928−1936.

(9) Raffaini, G.; Ganazzoli, F. Surface Ordering of Proteins Adsorbed on Graphite. *J. Phys. Chem. B* **2004**, *108*, 13850−13854.

(10) Mücksch, C.; Urbassek, H. M. Molecular Dynamics Simulation of Free and Forced BSA Adsorption on a Hydrophobic Graphite Surface. *Langmuir* **2011**, *27*, 12938−12943.

(11) Mücksch, C.; Rösch, C.; Müller-Renno, C.; Ziegler, C.; Urbassek, H. M. Consequences of Hydrocarbon Contamination for Wettability and Protein Adsorption on Graphite Surfaces. *J. Phys. Chem. C* **2015**, *119*, 12496−12501.

(12) De Leo, F.; Magistrato, A.; Bonifazi, D. Interfacing proteins with graphitic nanomaterials: from spontaneous attraction to tailored assemblies. *Chem. Soc. Rev.* **2015**, *44*, 6916−6953.

(13) Iijima, S. Helical microtubules of graphitic carbon. *Nature* **1991**, *354*, 56−58.

(14) Mtsuko, D.; Koshio, A.; Yudasaka, M.; Iijima, S.; Ahlskog, M. Measurements of the transport gap in semiconducting multiwalled carbon nanotubes with varying diameter and length. *Phys. Rev. B: Condens. Matter Mater. Phys.* **2015**, *91*, 195426.

(15) Laitinen, O. H.; Nordlund, H. R.; Hytönen, V. P.; Kulomaa, M. S. Brave new (strept)avidins in biotechnology. *Trends Biotechnol.* **2007**, *25*, 269−277.

(16) Hytönen, V. P.; Määttä, J. A. E.; Nyholm, T. K. M.; Livnah, O.; Eisenberg-Domovich, Y.; Hyre, D.; Nordlund, H. R.; Hörhä, J.; Niskanen, E. A.; Paldanius, T.; et al. Design and construction of highly stable, protease-resistant chimeric avidins. *J. Biol. Chem.* **2005**, *280*, 10228−10233.

(17) Hokkanen, M. J.; Lautala, S.; Shao, D.; Turpeinen, T.; Koivistoinen, J.; Ahlskog, M. On-chip purification via liquid immersion of arc-discharge synthesized multiwalled carbon nanotubes. *Appl. Phys. A: Mater. Sci. Process.* **2016**, *122*, 634.

(18) Livnah, O.; Bayer, E. A.; Wilchek, M.; Sussman, J. L. Three-dimensional structures of avidin and the avidin-biotin complex. *Proc. Natl. Acad. Sci. U.S.A.* **1993**, *90*, 5076−5080.

(19) Reichert, J.; Wei, G.; Jandt, K. D. Formation and Topotactical Orientation of Fibrinogen Nanofibrils on Graphite Nanostructures. *Adv. Eng. Mater.* **2009**, *11*, B177−B181.

(20) Izrailev, S.; Stepaniants, S.; Balsera, M.; Oono, Y.; Schulten, K. Molecular dynamics study of unbinding of the avidin-biotin complex. *Biophys. J.* **1997**, *72*, 1568−1581.

(21) Wang, J.; Dixon, R.; Kollman, P. A. Ranking ligand binding affinities with avidin: a molecular dynamics-based interaction energy study. *Proteins: Struct., Funct., Bioinf.* **1999**, *34*, 69−81.

(22) Söderhjelm, P.; Kongsted, J.; Ryde, U. Ligand Affinities Estimated by Quantum Chemical Calculations. *J. Chem. Theory Comput.* **2010**, *6*, 1726−1737.

(23) Macwan, I.; Khan, M. D. H.; Aphale, A.; Singh, S.; Liu, J.; Hingorani, M.; Patra, P. Interactions between avidin and graphene for development of a biosensing platform. *Biosens. Bioelectron.* **2017**, *89*, 326−333.

(24) Barinov, N. A.; Prokhorov, V. V.; Dubrovin, E. V.; Klinov, D. V. AFM visualization at a single-molecule level of denaturated states of proteins on graphite. *Colloids Surf., B* **2016**, *146*, 777−784.

(25) Zauner, D.; Taskinen, B.; Eichinger, D.; Flattinger, C.; Ruttmann, B.; Knoglinger, C.; Traxler, L.; Ebner, A.; Gruber, H. J.; Hytönen, V. P. Regenerative biosensor chips based on switchable mutants of avidin-A systematic study. *Sens. Actuators, B* **2016**, *229*, 646−654.

(26) Herrig, A.; Janke, M.; Austermann, J.; Gerke, V.; Janshoff, A.; Steinem, C. Cooperative Adsorption of Ezrin on PIP2-Containing Membranes†. *Biochemistry* **2006**, *45*, 13025−13034.

(27) Helbing, C.; Stoeßel, R.; Hering, D. A.; Arras, M. M. L.; Bossert, J.; Jandt, K. D. pH-Dependent Ordered Fibrinogen Adsorption on Polyethylene Single Crystals. *Langmuir* **2016**, *32*, 11868−11877.

(28) Lin, Y.; Allard, L. F.; Sun, Y.-P. Protein-Affinity of Single-Walled Carbon Nanotubes in Water. *J. Phys. Chem. B* **2004**, *108*, 3760−3764.

(29) Karajanagi, S. S.; Yang, H.; Asuri, P.; Sellitto, E.; Dordick, J. S.; Kane, R. S. Protein-Assisted Solubilization of Single-Walled Carbon Nanotubes. *Langmuir* **2006**, *22*, 1392−1395.

DOI: 10.1021/acs.langmuir.8b02855
Langmuir 2018, 34, 15335−15342

(30) Mu, Q.; Liu, W.; Xing, Y.; Zhou, H.; Li, Z.; Zhang, Y.; Ji, L.; Wang, F.; Si, Z.; Zhang, B.; et al. Protein Binding by Functionalized Multiwalled Carbon Nanotubes Is Governed by the Surface Chemistry of Both Parties and the Nanotube Diameter. *J. Phys. Chem. C* **2008**, *112*, 3300−3307.
(31) Balavoine, F.; Schultz, P.; Richard, C.; Mallouh, V.; Ebbesen, T. W.; Mioskowski, C. Helical Crystallization of Proteins on Carbon Nanotubes: A First Step towards the Development of New Biosensors. *Angew. Chem., Int. Ed.* **1999**, *38*, 1912−1915.
(32) Ling, W. L.; Biro, A.; Bally, I.; Tacnet, P.; Deniaud, A.; Doris, E.; Frachet, P.; Schoehn, G.; Pebay-Peyroula, E.; Arlaud, G. J. Proteins of the Innate Immune System Crystallize on Carbon Nanotubes but Are Not Activated. *ACS Nano* **2011**, *5*, 730−737.
(33) Tapio, K.; Shao, D.; Auer, S.; Tuppurainen, J.; Ahlskog, M.; Hytönen, V. P.; Toppari, J. J. A DNA nanoparticle actuator enabling optical monitoring of nanoscale movements induced by an electric field. *Nanoscale* **2018**, *10*, 19297−19309.
(34) Taskinen, B.; Zauner, D.; Lehtonen, S. I.; Koskinen, M.; Thomson, C.; Kähkönen, N.; Kukkurainen, S.; Määttä, J. A. E.; Ihalainen, T. O.; Kulomaa, M. S.; et al. Switchavidin: Reversible Biotin-Avidin-Biotin Bridges with High Affinity and Specificity. *Bioconjugate Chem.* **2014**, *25*, 2233−2243.

DOI: 10.1021/acs.langmuir.8b02855
Langmuir 2018, 34, 15335−15342